Short fiber reinforced composites: unbiased full-field evaluation of various homogenization methods in elasticity

C. Naili[1], *I. Doghri*[1*], *T. Kanit*[2], *M.S. Sukiman*[2,4], *A. Aissa − Berraies*[3], *A. Imad*[2]

[1] *Université catholique de Louvain, Institute of Mechanics, Materials and civil Engineering (IMMC) Baîtiment Euler, 4 Avenue G. Lemaitre, B-1348 Louvain-La-Neuve, Belgium.*

[2] *Unité de Mécanique de Lille, Univ. Lille, F-59000 Lille, France*

[3] *Department of Civil Engineering and Architecture, University of Pavia, Italy*

[4] *Center of Advanced Materials, Department of Mechanical Engineering, Faculty of Engineering, University of Malaya, Malaysia.*

Abstract

This paper deals with the evaluation of several homogenization methods for short fiber-reinforced composites (SFRC) in isothermal linear elasticity. In order to have an unbiased assessment, only full-field finite element (FE) versions of the methods are developed and studied, no analytical mean-field models are considered. Firstly, the FE homogenization of unidirectional (UD) SFRC is performed using two computational models: representative volume elements (RVE) and unit cells, and comparing their predictions. Secondly, for the homogenization of misaligned SFRC, a model RVE seen as an aggregate of UD pseudo-grains (PG) is homogenized in two steps. In the first step, the effective response of PGs is obtained by FE analysis on UD unit cells. The second step is performed with one of three homogenization schemes: Voigt, Reuss and a FE-based version of the Mori-Tanaka (MT) model. The latter is equivalent to a direct MT homogenization of the RVE. The actual SFRC microstructure is 3D, but because of limited computer resources, the current article is restricted to 2D analyses, which nevertheless provide some guidance. A parametric study is conducted using several fiber volume fractions and orientation tensor components. Both the effective properties of RVEs and the mean strains inside individual fibers are assessed against reference results obtained by direct FE homogenization of the actual RVEs.

Keywords:
Short-fiber-reinforced-composite; Modeling; Computational simulation; Homogenization

1. Introduction

Nowadays, short fiber reinforced composites (SFRC) represent numerous industrial applications. This composite material is usually made of short glass fibres embedded in a thermoplastic polymer matrix in linear isothermal elasticity. The main manufacturing process is injection molding which enables a large scale production of SFRC parts. This process leads

*Corresponding author. Tel: Tel. (+32-10-47)8042, (...)2350, Fax (...)2180.
E-mail adresses: chiheb.naili@uclouvain.ve (C. Naili), issam.doghri@uclouvain.be (I. Doghri).

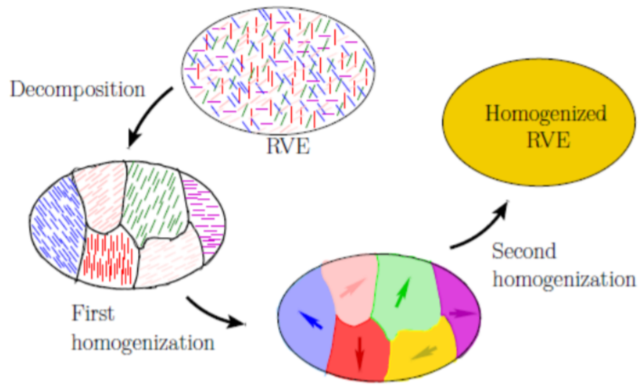

Figure 1: Pseudo-grain decomposition and two-step homogenization method. Actual RVE (top). A model RVE (left) is viewed as a set of pseudo-grains (PG). Each one of them is homogenized separately (step 1), then the aggregate of homogeneous PGs is homogenized (step 2) (Kammoun. et al.)[5].

to a considerable variation of the fibers' length and orientation within a part and even inside each small volume of a part. Therefore the material response is both strongly anisotropic and heterogeneous throughout a part, which explains why modeling these characteristics can be difficult and challenging. This is where micromechanical approaches come to be so effective since they enable the computation of the macro stress and strain fields in a composite part based on the local (micro) response of each phase. In fact, one could solve representative volume element (RVE) problems using direct full-field methods, e.g. finite element (FE) analysis. However these full-field RVE simulations are costly in terms of both CPU and users' time. An alternative solution which is much easier and computationally cheaper by several orders of magnitude is based on mean-field (MF) homogenization methods. For misaligned SFRC, a method which became classical is the pseudo-grain decomposition followed by two-step homogenization (Camacho et al. [1] ; Lielens [2] ; Lusti and Gusev [3] ; Pierard et al. [4]). Accordingly see (fig.1), a model RVE is decomposed into unidirectional (UD) pseudo-grains (PG) where each PG is made of identical aligned fibers embedded in the matrix. Each PG is homogenized using a MF model, typically Mori-Tanaka (MT) [6]. Next, in the second step, the RVE seen as an aggregate of PGs is homogenized with MF, typically a simple Voigt scheme. It is also possible to homogenize the initial RVE (matrix with misaligned fibers) directly with MF, typically MT, e.g (Pierard et al. [4] ; Jain et al. [7]). Today MF homogenization of SFRC, based on the two-step method or a direct MT one, is widely used in the literature, and also in commercial software. For this reason, several works aiming to study the accuracy of MF predictions by comparison to full-field calculations have been conducted. For example, Müller et al. [8] determined the effective linear elastic properties of SFRC by MF and full-field fast Fourier transform and found deviations between both approaches to increase with phase contrast and fiber volume fraction. Lobos Fernández and Böhlke [9] provided methods to present and compute the Hashin-Shtrikman bounds for linear anisotropic elastic polycrystalline materials. Studies were also conducted in order to determine the distribution orientation tensors that adequately describe the composites e.g. Tseng et al.[30] and conclude whether a second or a fourth order tensor is sufficient e.g., Müller and Böhlke [10]. Experimental studies based on X-ray micro-computed tomography

that rely on an iterative single fiber segmentation and merging procedure to obtain the fiber characteristics (orientation, location, radius and length) were also conducted by Hessman et al.[11] . To keep the deviations lower than 10%, a maximum contrast and fiber volume fraction of 44 and 17% are recommended. Tian et al. [12] modified the two-step method based on the Voigt and Reuss models to obtain excellent correlation with RVE based FE method on effective elastic properties of short fiber-reinforced metal matrix composites. Another similar paper by Tian et al. [13] concluded that the two-step MF homogenization produced the same results as the FE simulations but the former has the advantage of demanding less computational processing power. On the other hand, Jain et al [7]. found that the two-step method with Voigt in the second step leads to poor predictions of average stresses in individual fibers while the direct MT method yielded better consistency with FE results.
The main goal of the present contribution is to conduct an unbiased evaluation of various homogenization schemes using only full-field FE simulations and not analytical MF models such as MT. This will enable in particular to assess two-step methods against direct homogenization. As a preliminary, the effective response of a UD unit cell is assessed against an RVE with UD fibers, with FE homogenization in both cases. Next, the response of misaligned SFRCs is evaluated using two schemes, one that homogenizes an RVE directly with FE computation and another one that uses a two-step method. The latter takes into account the FE predicted effective properties of a UD unit cell in the first step and uses three different homogenization methods in the second step: Voigt, Reuss and a model that is inspired by direct MT. The latter scheme is shown to enter within the two-step methodology.
The paper has the following outline. In sect. 2, a comparison between an RVE model and a unit-cell for UD fibers is conducted. In sect. 3 different two-step schemes based on FE homogenization for misaligned fibers are developed, investigated and compared to reference direct FE simulations on RVE. Conclusions are drawn in sect. 4. Mathematical details regarding the proposed methods are given in Appendix A.

Acronyms: SFRC: Short Fiber Reinforced Composite, BC: Boundary Condition, FE: Finite Element, MF: Mean Field, MT: Mori-Tanaka, PG: Pseudo-Grain, RVE: Representative Volume Element, UD: Unidirectional.

2. Unidirectional (UD) fibers

2.1. Finite element homogenization with RVE model

2.1.1. RVE generation

The microstructures are generated using Digimat-FE [14] with randomly positioned fibers, oriented along the x-axis. The fibers' aspect ratio is 24. The size of the microstructures is set at 200 x 200 in comparison to a fiber length of 24. This size is large enough to be a Representative Volume Element (RVE), which ensures no bias in the calculations even with different boundary conditions (BC). Leclerc and Karamian-Surville [15] explain that the RVE needs to be five times larger than the fibers' length, while Harper et al. [16] stated that it should be four times larger. Microstructures with three different fiber volume fractions (v_f) are illustrated in Figure 2. For each case, 5 realizations, each corresponding to a random distribution of fibers positions are simulated and the realization-averaged results are computed and reported. Small standard deviations indicated little variations in the results between the different realizations.

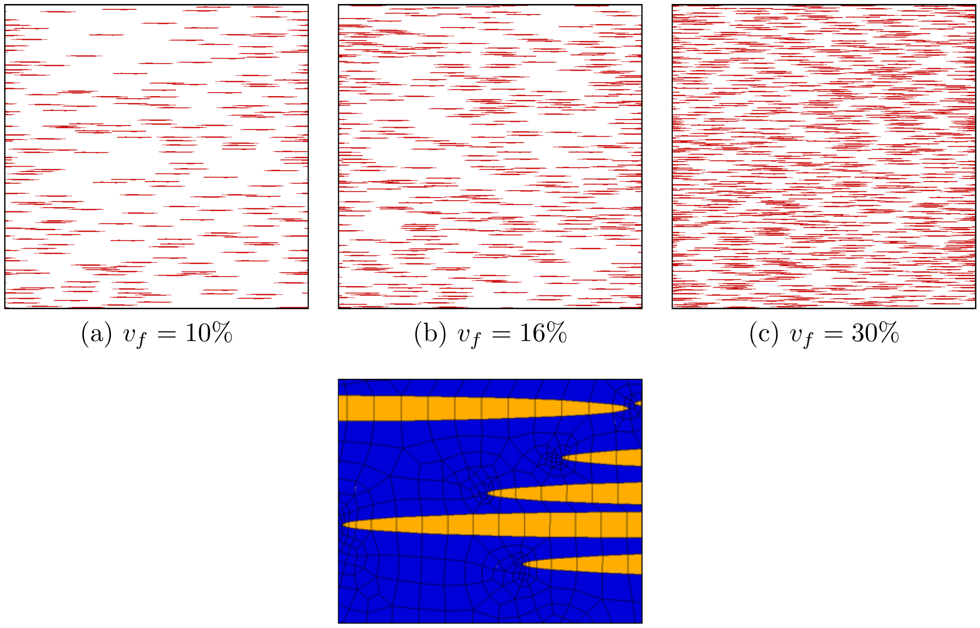

(a) $v_f = 10\%$ (b) $v_f = 16\%$ (c) $v_f = 30\%$

(d) Zoom on the fibers

Figure 2: Different microstructures for the case of aligned fibers with varying volume fraction v_f.

2.1.2. Finite element meshing

The previous microstructures are meshed using the free meshing technique to perform the finite element (FE) calculations using the Abaqus solver [17] . As opposed to the multi-phase meshing technique with regularly distributed square elements, the free meshing technique follows precisely the shape of inclusions in the microstructure. In principle, this leads to better accuracy in the FE calculations; e.g. Lippmann et al. [18] studied the differences between the two meshing techniques. The free mesh here is composed of 4-noded quadrilateral elements with reduced integration (C2D4R in Abaqus) and 3-noded triangular elements with complete integration (C2D3). The latter are concentrated mostly around sharp fiber edges while the quadrilateral elements cover the majority of the microstructures. The free mesh is already optimized to ensure a good precision of calculations, however, a study on mesh density is required to observe if the free mesh has a sufficient number of elements. Simple tensile tests along the fibers' direction are carried out. For each volume fraction and each mesh density, 5 realizations of random fiber locations are simulated, and the realisation-averaged results are computed. Tables 1 and 2 show the relative error between mean stress $\langle \sigma_{11} \rangle$ computed after 5 different realisations with different mesh densities for 2 volume fractions $v_f = 16\%$ and 30%. The results for $v_f = 30\%$ stabilize at 96237 elements. As for $v_f = 16\%$, the relative difference does not exceed 0.57% which proves that even the coarsest mesh is efficient enough for our calculations. By taking into account the previous case, the chosen mesh density is around 90000 elements for all calculations.

Number of elements	39838	96237	135045
Relative difference (%)	3.95	0.15	

Table 1: Tension test in direction 1. Accuracy in mean stress $\langle \sigma_{11} \rangle$ prediction for different mesh densities for $v_f = 30\%$

Number of elements	27883	83802	162224
Relative difference (%)	0.57	0.14	

Table 2: Tension test in direction 1. Accuracy in mean stress $\langle \sigma_{11} \rangle$ prediction for different mesh densities for $v_f = 16\%$.

The number of fibers for $v_f = 30\%$ is 633 and the fibers do not touch each other. For the chosen mesh density, around 30200 elements are located on all the fibers, which means that each fiber possesses around 48 elements.

2.1.3. Boundary conditions

In a 2D problem, the matrix representation of Hooke's law is simplified as follows (where $\bar{\sigma}_{ij}$ and $\bar{\varepsilon}_{ij}$ are the macroscopic stress and strain components) :

$$\begin{bmatrix} \bar{\sigma}_{11} \\ \bar{\sigma}_{22} \\ \bar{\sigma}_{12} \end{bmatrix} = \begin{bmatrix} \bar{C}_{11} & \bar{C}_{12} & \bar{C}_{16} \\ \bar{C}_{12} & \bar{C}_{22} & \bar{C}_{26} \\ \bar{C}_{16} & \bar{C}_{26} & \bar{C}_{66} \end{bmatrix} \begin{bmatrix} \bar{\varepsilon}_{11} \\ \bar{\varepsilon}_{22} \\ 2\bar{\varepsilon}_{12} \end{bmatrix} \tag{1}$$

Three different computations are carried out to determine the full stiffness matrix. For example, to find the first column, this macroscopic strain is applied:

$$\bar{\varepsilon} = \begin{bmatrix} \bar{\varepsilon}_{11} \\ 0 \\ 0 \end{bmatrix} \tag{2}$$

The engineering properties are then computed from $[\bar{C}]$. The strain tensor is integrated into a Dirichlet type BC called Kinetic Uniform BCs (KUBC). A previous study done by Kanit et al. [19] shows that the convergence of apparent properties is obtained faster with periodic BCs (PBC) than with Dirichlet types like KUBC. However, the mesh used in this study is a free mesh with uneven node distributions along the edges of the microstructure. This makes it difficult for each node to find its homologous point, which is a prerequisite in the application of PBC. Nevertheless, the generated microstructures in this study are considered RVE, therefore the calculated properties will not depend on the type of BCs used. The KUBC applied here should produce effective properties of the composite.

Consider the 2D microstructure S, the KUBC is applied by imposing a uniform strain $\bar{\varepsilon}$ at points x which belong to the boundary ∂S :

$$u = \bar{\varepsilon} \cdot x \quad \forall x \in \partial S \tag{3}$$

The calculations done in the RVE study are under a plane stress hypothesis. The results are shown in the next sections with comparisons with those of unit cells.

2.2. Finite element homogenization with unit cell model

In this section we discuss a simpler alternative to the RVE, that is a 2D unit cell that contains a periodic distribution of a few fibers embedded in matrix phase.

2.2.1. Unit cell generation

The volume fraction of the fibers v_f and the matrix v_m are given as :

$$v_f = \frac{2ld}{LD}; \qquad v_m = 1 - v_f \tag{4}$$

with l and d the fibers' length and width, resp.; L and D the cell's length and width resp.; see figure 3. Knowing the fibers' width d and aspect ratio $A_r = \frac{l}{d}$, their length l is computed. In order to compute the rest of the parameters we added the following assumption (Kang and Gao [20]) :

$$L - D = l - d \tag{5}$$

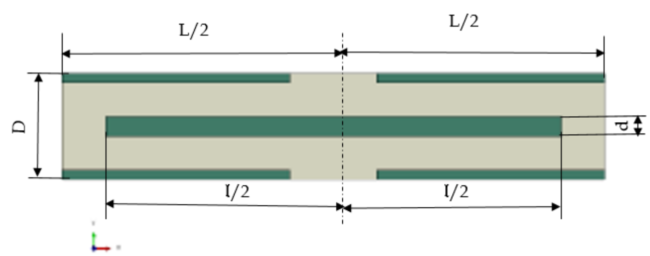

Figure 3: Geometry of the 2D unit cell model.

2.2.2. Boundary conditions

We used periodic boundary conditions (PBC) [21] such that

$$u^+ - u^- = \bar{\varepsilon}.(x^+ - x^-) \tag{6}$$

where u^+ , u^- , x^+ and x^- are the displacements and the point coordinates of pairs of "homologous" edges. For the mesh, we used two different types of elements in Abaqus: CPS8R (an 8-node biquadratic plane stress quadrilateral, reduced integration) and CPE8R (an 8-node biquadratic plane strain quadrilateral, reduced integration). In the post processing, we compute the stress and strain fields in the fibers and matrix phases separately and we calculate the macro stress as the volume average over the cell :

$$\overline{\sigma}_{ij} \equiv < \sigma_{ij} > \equiv \frac{1}{V}\int_V \sigma_{ij} dV \quad ; \quad \overline{\varepsilon}_{ij} = < \varepsilon_{ij} > \equiv \frac{1}{V}\int_V \varepsilon_{ij} dV \tag{7}$$

In order to compute the engineering properties, 3 different tests are performed :

– a tension test along the fiber direction that enables to compute the Young's modulus in that direction and Poisson's ratio, since $\overline{E}_1 = \frac{\overline{\sigma}_{11}}{\overline{\varepsilon}_{11}}$ and $\bar{v}_{12} = -\frac{\overline{\varepsilon}_{22}}{\overline{\varepsilon}_{11}}$;
– a tension test normal to the direction of the fibers in order to compute the Young's modulus along that direction and Poisson's ratio, since $\overline{E}_2 = \frac{\overline{\sigma}_{22}}{\overline{\varepsilon}_{22}}$ and $\bar{v}_{21} = -\frac{\overline{\varepsilon}_{11}}{\overline{\varepsilon}_{22}}$;
– a shear test that enables to compute the shear modulus, since $\overline{G}_{12} = \frac{\overline{\sigma}_{12}}{2\overline{\varepsilon}_{12}}$.
For each unit cell model we used a number of elements equal to 30000. To study the effect of mesh density, models with finer mesh, 45000 and 60000 elements, were created. For each mesh density, the exact same effective properties were found (Table 3) and the same local line values (figures 4 to 6).

2.3. Comparison between RVE and unit cell results

In this section we present results of numerical simulations and compare the effective engineering properties obtained with the two FE models: RVE and unit cell. The elastic properties used for the matrix and the fibers are: $E_m = 3.1\ GPa$; $\nu_m = 0.35$; $E_f = 76\ GPa$; $\nu_m = 0.22$. The fibers' aspect ratio is $A_r = 24$ and we tested 3 volume fractions (10%,16% and 30%). The chosen data is typical of short glass fiber reinforced thermoplastic polymers.

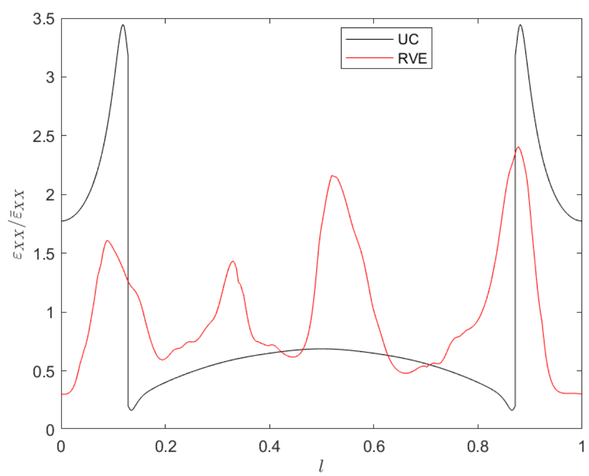

Figure 4: UD unit cell and RVE:strain ε_{XX} evolution along a path for a tension test along the fiber direction $v_f = 16\%$.

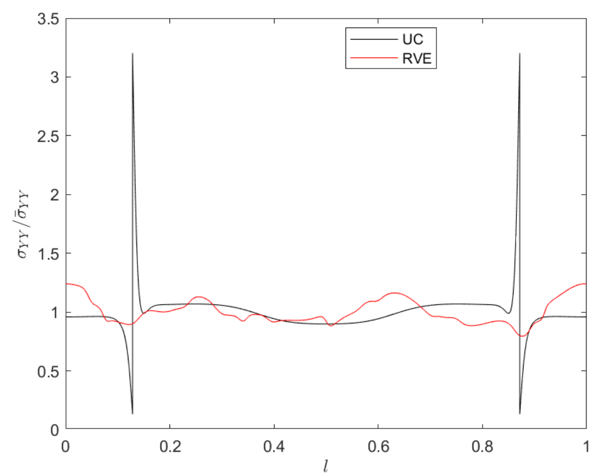

Figure 5: UD unit cell and RVE: stress σ_{YY} [MPa] evolution along a path for a tension test normal to the fiber direction $v_f = 16\%$.

First, for $v_f = 16\%$ and for the unit cell of Fig. 3, we report results along a path which is initially a horizontal line cutting through the middle of the cell .These results are compared to those of RVE of Fig.2 . For a tension test in the fiber direction, Fig. 4 shows that for both models the axial strains are not uniform, and therefore a Voigt assumption is invalid, contrarily to the case of continuous fiber reinforced composites. For a tension test in a direction normal to the fibers, Fig. 5 shows that except at the interfaces between the matrix and fiber tips, a Reuss model assuming uniform transverse stress is acceptable. Finally, for a shear test, Fig. 6 shows that the shear stresses are not uniform along the path, and thus a Reuss assumption is invalid. One reason for the different results between the unit cell and the RVE models in figures 4 to 6 is that the fibers are represented by rectangles in the

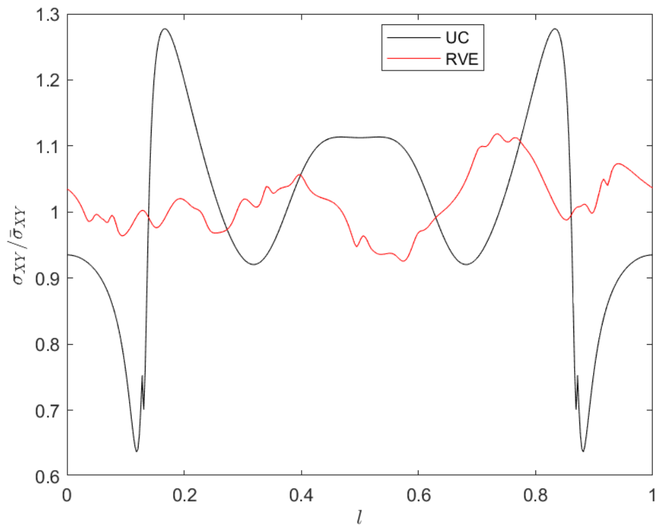

Figure 6: UD unit cell and RVE: stress σ_{YY} [MPa] evolution along a path for a shear test $v_f = 16\%$.

former model and by ellipses in the latter (because of Digimat-FE limitations). In order to investigate further the strain heterogeneity inside the entire unit cell for a tension test along the fibers' direction, we computed the cumulative probability that the axial strain is lower than a given value. The strain at each Gauss point of the mesh is considered as well as the corresponding volume (or area). Figure 7 shows that the axial strain field is strongly heterogeneous inside the unit cell, since the cumulative probability curve is significantly wide around the mean axial strain value represented by the vertical line. This proves again that a Voigt rule of mixture is invalid.

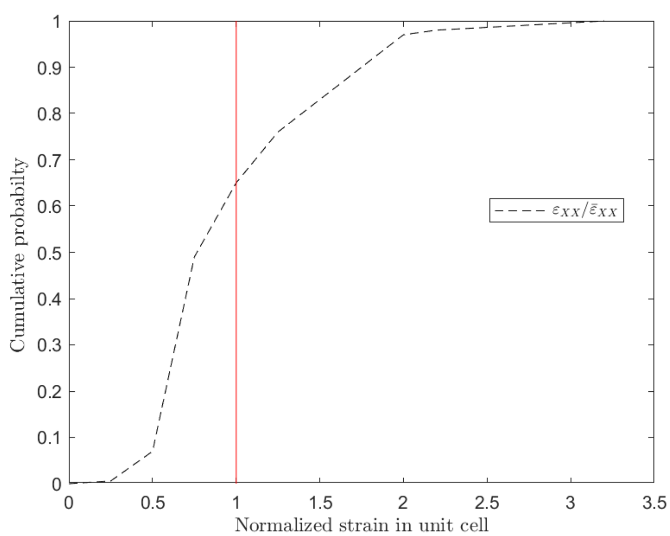

Figure 7: Cumulative probabilities inside the entire unit cell of the normalized axial strain under a tensile loading along the fibers' direction for a fibers' volume fraction of 16%

Table 3 reports the normalized effective engineering properties obtained with the two FE models (RVE and unit cell) for fiber volume fractions of 10%, 16% and 30%, resp.

	RVE	Unit cell	Error(%)
$\frac{\overline{E}_1}{E_m}$	2.12	2.08	1.72
	2.94	3.01	2.44
	5.33	5.38	0.99
$\frac{\overline{E}_2}{E_m}$	1.18	1.17	1.01
	1.29	1.28	0.61
	1.57	1.58	0.33
$\frac{\overline{G}_{12}}{G_m}$	1.12	1.14	1.72
	1.21	1.22	1.14
	1.46	1.43	2.34
$\frac{\overline{\nu}_{12}}{\nu_m}$	1.01	1.04	3.38
	0.98	0.98	0.17
	0.97	0.91	6.65

Table 3: UD composite: plane stress results. For each effective property there are 3 rows corresponding to $v_f = 10\%$, 16% and 30%, resp.

Table 3 shows an excellent agreement between the effective properties predicted by the two FE models since for all the volume fractions the relative error is less then 3.38% except for one at 6.65%.

Because of limited computer resources, the current article is restricted to 2D studies, which nevertheless provide some guidance. However, the actual SFRC microstructure is 3D, and clearly for quantitative estimates of effective properties, 2D models are insufficient. We carried out 3D FE simulations using two different unit cell models (figures 8 and 9), one was created with Digimat-FE that defines the fibers as cylinders with hemispherical end caps and the second one after Levy and Papazian [24] where fibers are cylinders. A significant difference between the two models is that fiber overlapping for the Digimat-FE 3D unit cell is not as important as in the second model. We used the same aspect ratio $A_r = 24$ as in the 2D case for both models. The 3D cell created by Digimat-FE has a length $L = 47.6$, a width $D = 4.11$ and a thickness $e = 2.37$, and the second model has $L = 32.3$, a width $D = 9.3$ and a thickness $e = 9$. As for the mesh we used 36665 elements of type C3D10 in Abaqus (a 10 node quadratic tetrahedron) for the model created with Digimat-FE, as for the second model we used 54432 elements of type C3D8R (An 8-node linear brick). The results are compared with those of 2D plane stress and also 2D plane strain unit cells, in Table 4 for $v_f = 16\%$.

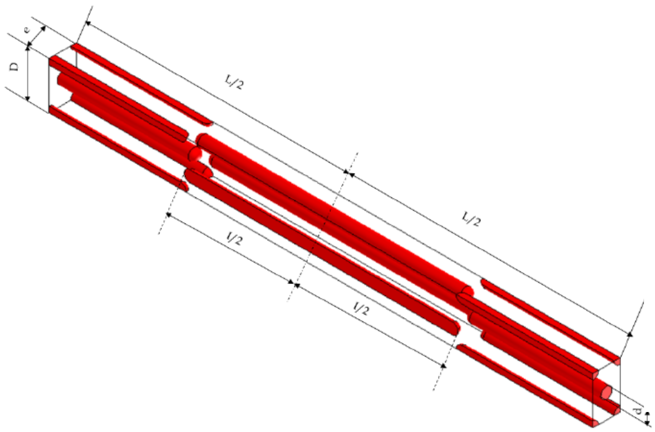

Figure 8: UD composite: 3D unit cell model with Digimat-FE.

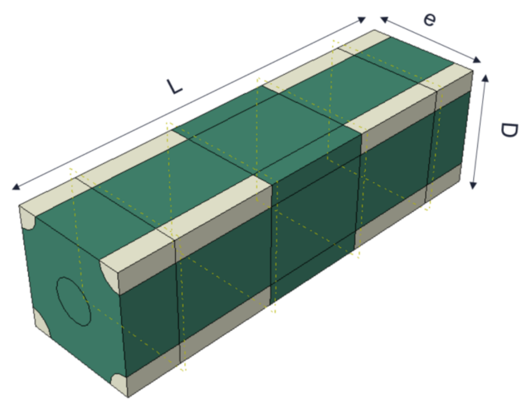

Figure 9: UD composite: 3D unit cell model by Levy and Papazian [24].

	2D plane stress	2D plane strain	Digimat 3D unit cell	Levy and Papazian 3D unit cell
$\frac{\overline{E}_1}{E_m}$	3.01	3.2	3.9	2.7
$\frac{\overline{E}_2}{E_m}$	1.28	1.64	1.38	1.32
$\frac{\overline{G}_{12}}{G_m}$	1.22	1.14	1.4	1.3

Table 4: Comparison between 2D and 3D unit cell results for fibers' volume fraction $v_f = 16\%$

The effective properties for 3D and 2D plane strain were calculated using the same tests as in Sect. 2.2.2. However, the effective moduli $\bar{E}_1$ and $\bar{E}_2$ computed for 2D plane strain cannot be interpreted in the same way as in 2D plane stress. This is due to a non-zero stress along the out-of-plane direction after doing a tensile test in directions 1 or 2. From table 4 we can see that the two 3D unit cells do not predict the same effective properties and that generally the 3D predictions do not lie between 2D plane stress and 2D plane strain. Table 4 results are provided for information only, as to our knowledge, such a bracketing is not expected for SFRC.

Finally, we investigated the validity of eq.(5), a basic assumption for the 2D unit cell. We first checked whether the equation is verified for the RVE, so average distances L_{avg} and D_{avg} between fibers were computed for RVE with $v_f = 10\%$ (see figure 10). We found that for the RVE, $L_{avg} - D_{avg} = 1.8(l - d)$. Next we created a unit cell model with the same volume fraction considering also $L - D = 1.8(l - d)$. Table 5 shows that for this case the relative error for the Young's modulus along the fibers' direction is equal to 4.2%, which is too high compared to unit cell with the original eq.(5), see table 3 (although the accuracy improves for other engineering constants). The issue is unclear, and might be due to the fibers being modeled as rectangles in the unit cell and ellipses in the RVE model (due to

Digimat-FE software limitations). In subsequent computations, we kept eq.(5) for the unit cell.

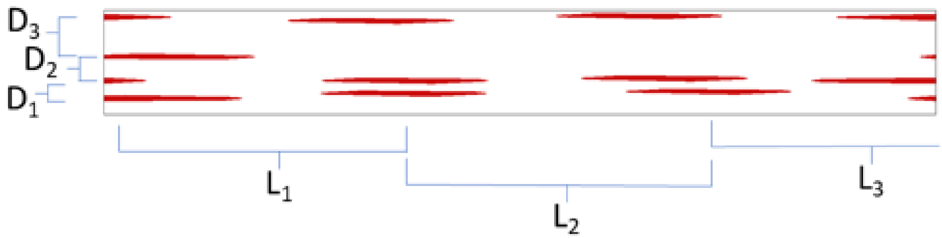

Figure 10: RVE with aligned fibers. Computation of average distances L_{avg} and D_{avg} between fibers

	UD unit cell	RVE	Error(%)
$\frac{\overline{E}_1}{E_m}$	2.21	2.12	4.2
$\frac{\overline{E}_2}{E_m}$	1.18	1.18	0.006
$\frac{\overline{G}_{12}}{G_m}$	1.11	1.12	0.8
$\frac{\overline{\nu}_{12}}{\nu_m}$	1.00	1.01	0.7

Table 5: UD composite: plane stress results for fibers' volume fraction $v_f = 10\%$ for a unit cell such that $L - D = 1.8(l - d)$

.

3. Misaligned fibers

In this section we study several homogenization strategies for a composite material reinforced with misaligned short fibers which have the same material and aspect ratio but different orientations.

3.1. Orientation distribution function and orientation tensor

We designate by $\overrightarrow{p}$ the unit vector along a fiber's axis, $\Psi(\overrightarrow{p})$ is the orientation distribution function (ODF) and $\mathbf{a}$ is the second-order symmetric orientation tensor (OT). The ODF verifies :

$$\oint \Psi(\overrightarrow{p})\, dw_p = 1 \quad ; \quad \Psi(\overrightarrow{p}) = \Psi(\overrightarrow{-p}) \tag{8}$$

and gives the probability to find fibers within orientations $\overrightarrow{p}$ and $(\overrightarrow{p} + d\overrightarrow{p})$. In 3D dw_p designates the infinitesimal surface area (resp. arc length) on the unit sphere (resp. unit circle). The OT gives a measure of the average fiber orientation in the RVE, and is defined as:

$$a_{ij} = \oint p_i p_j \Psi(\overrightarrow{p})\, dw_p \;\equiv\; < p_i p_j >_\Psi \tag{9}$$

In 2D, we consider a global (fixed) Cartesian system (O,X,Y). Special cases are : $a_{11} = 1$ and $a_{11} = 0$ (fibers aligned along (O,X) and (O,Y) axes, resp.) and $a_{11} = a_{22} = \frac{1}{2}$ (2D random orientation in the (O,X,Y) plane); see figure 11.
If we consider that ϕ is the angle between a single fiber and the X-axis; then:

$$\overrightarrow{p} = \begin{bmatrix} \cos\phi \\ \sin\phi \end{bmatrix} \quad ; \quad \int_0^{2\pi} \Psi(\phi)\, d\phi = 1 \quad ; \quad a_{ij} = \int_0^{2\pi} p_i p_j \Psi(\phi)\, d\phi \tag{10}$$

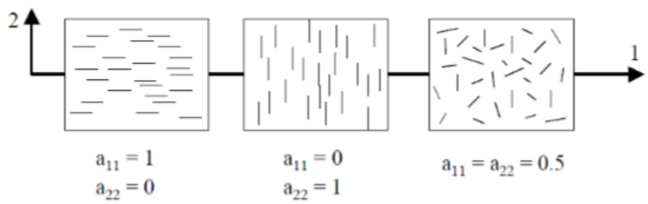

Figure 11: Orientation of the fibers in function of the OT components.

3.2. Direct FE on RVE

The direct calculation method on RVE used previously for aligned fibers is implemented here on misaligned fibers. Digimat-FE has a built-in function which allows the designation of the ODF. The value of a_{11} is varied between 0.5 and 0.8 for fibers' volume fraction $v_f =$ 0.10 and 0.16. The size of the microstructures is kept at 200×200 as in section 2.1 to ensure that they are indeed RVE and to retain coherence with the previous calculations. Examples of the generated microstructures are shown in Figure 12 for $v_f = 0.10$ with different values of a_{11}. Similar microstructures were generated for $v_f = 0.16$, but this became impossible when v_f reached 0.30. As the number of fibers increases, v_f reaches the so-called percolation threshold; i.e. the v_f value at which the fiber contacts start to appear. The threshold is also dependent on the fiber geometry and orientation. Balberg et al. [26] used the excluded volume method to calculate the percolation threshold based on fiber parameters. As the number of degrees of freedom increases when a_{11} approaches 0.5, the possibility of contact between fibers also increases. Consequently, the microstructure generation for $v_f = 0.30$ is only achievable in the case of $a_{11} = 0.8$ where the majority of the fibers follows one direction. The mesh and the BCs are identical to the case of aligned fibers in section 2.1

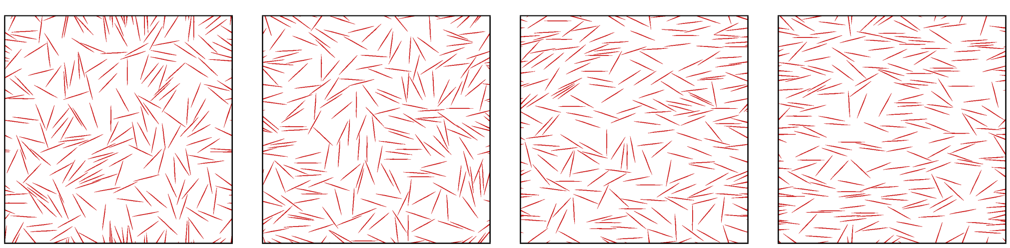

(a) $a_{11} = 0.5$ (b) $a_{11} = 0.6$ (c) $a_{11} = 0.7$ (d) $a_{11} = 0.8$

Figure 12: Different microstructures for fibers' volume fraction $v_f = 0.10$ varying the OT component a_{11}

as convergence of calculations is already expected. For each case 5 random realizations are created and simulated and the realization-averaged results are computed and reported in the following.

3.3. Pseudo-grain decomposition and two-step homogenization

The general concept behind a two-step homogenization method is based on decomposing a model RVE into multiple pseudo grains (PG). Each PG is made of a matrix material reinforced with fibers with the same direction, shape and aspect ratio. Next, homogenization proceeds in two steps: for each PG (Step 1) and for the aggregate of PG (Step 2). The two-step method is illustrated in figure 1. In the first step, each PG is a two-phase composite which contains a matrix and fibers with the same orientation and aspect ratio. The effective engineering properties of the PG are those obtained by FE homogenization on the UD unit cells in sections 2.2 and 2.3. In the second step, the RVE is considered as an aggregate of homogenized PG (i), each one is characterized by a stiffness matrix $[\bar{\boldsymbol{C}}^{(i)}]$ and an orientation. Three homogenization methods are considered which differ only by the model assumed in the second step.

- First method: FE-Voigt

This model assumes that the strain field is uniform inside the aggregate. The macro stiffness matrix is computed as :

$$[\bar{\boldsymbol{C}}] =< [\bar{\boldsymbol{C}}(\overrightarrow{\boldsymbol{p}})] >_{\Psi} \approx \sum_i w_i [\bar{\boldsymbol{C}}^{(i)}] \tag{11}$$

To compute the stiffness matrix $[\bar{\boldsymbol{C}}^{(i)}\ ]$ of a PG (i), the UD cell's stiffness matrix is rotated from the local axes to the global ones. The weight of the orientation angle ϕ_i of a PG (i) is computed as:

$$w_i = 2\Psi(\phi_i)\Delta\phi \tag{12}$$

where $\Delta\phi$ is a fixed angle increment equal to 0.05 rad . All weights are normalized to ensure that $\sum_i w_i = 1$.

- Second method: FE-Reuss

This model assumes that the stress field is uniform in the aggregate. Consequently, the macro compliance matrix is obtained as :

$$[\bar{\boldsymbol{S}}] =< [\bar{\boldsymbol{S}}(\overrightarrow{\boldsymbol{p}})] >_{\Psi} \approx \sum_i w_i [\bar{\boldsymbol{S}}^{(i)}] \tag{13}$$

To compute the compliance matrix $[\bar{\boldsymbol{S}}^{(i)}\ ]$ of PG (i), the UD cell's compliance matrix is rotated from the local axes to the global ones.

- Third method : FE-MT

This model is based on FE homogenization inspired by Benveniste's interpretation [22] of Mori-Tanaka (MT) model [6]. According to Benveniste, the MT model can be interpreted as follows: each inclusion behaves as if it were isolated in an infinite matrix body subjected to a far field strain equal to the average matrix strain in the real RVE.

For misaligned inclusions, an interesting result is that a direct MT homogenization is just a special case of the two-step method. This result (Lielens, [2], Pierard et al., [4]) enables to write the main assumption of direct MT as follows:

$$< \boldsymbol{\varepsilon} >_{\omega^m_{\vec{p}}} = < \boldsymbol{\varepsilon} >_{\omega^m} \tag{14}$$

where ω^m and $\omega^m_{\vec{p}}$ designate the matrix domains in the RVE, and within a PG of orientation $\vec{p}$, resp. We designate by $\boldsymbol{B}^f_{\vec{p}}$ the partial strain concentration tensor (Dvorak and Benveniste, [27]) that relates the mean strains inside the fibers and the matrix within the PG:

$$< \boldsymbol{\varepsilon} >_{\omega^f_{\vec{p}}} = \boldsymbol{B}^f_{\vec{p}} :< \boldsymbol{\varepsilon} >_{\omega^m_{\vec{p}}} \tag{15}$$

The macro stiffness tensor predicted by direct MT is (see Appendix A):

$$\bar{\boldsymbol{C}} = (v_m \boldsymbol{C}^m + (1 - v_m) < \boldsymbol{C}^f : \boldsymbol{B}^f_{\vec{p}} >_\Psi) : (v_m \boldsymbol{I} + (1 - v_m) < \boldsymbol{B}^f{}_{\vec{p}} >_\Psi)^{-1} \tag{16}$$

Where $\boldsymbol{I}$ is the fourth-order symmetric identity tensor, $\boldsymbol{C}^f$ is the stiffness of the fibers and $\boldsymbol{C}^m$ is that of the matrix. An original contribution of this article is that we do not use the analytical formulae for MT model but we compute its partial concentration tensor using only FE homogenization of UD cells performed in section 2.2. Each PG is a two-phase composite where all fibers are identical, aligned of orientation $\vec{p}$ and embedded in a matrix. Using eq.(15) defining strain concentration tensor $\boldsymbol{B}^f_{\vec{p}}$ the effective stiffness of the PG is given by

$$\overline{\boldsymbol{C}}_{\vec{p}} = (v_m \boldsymbol{C}^m + (1 - v_m) \boldsymbol{C}^f : \boldsymbol{B}^f_{\vec{p}}) : (v_m \boldsymbol{I} + (1 - v_m) \boldsymbol{B}^f{}_{\vec{p}})^{-1} \tag{17}$$

Now $\bar{\boldsymbol{C}}_{\vec{p}}$ is obtained from FE analysis on a UD cell, the expression of $\boldsymbol{B}^f_{\vec{p}}$ is obtained as follows (see Appendix A, also Mayes and Hansen [28])

$$\boldsymbol{B}^f_{\vec{p}} = \frac{v_m}{1 - v_m} (\boldsymbol{C}^f - \overline{\boldsymbol{C}}_{\vec{p}})^{-1} : (\overline{\boldsymbol{C}}_{\vec{p}} - \boldsymbol{C}^m) \tag{18}$$

It is known that direct MT might lead to non-physical results, such as a non-diagonally symmetric effective stiffness matrix. The problem does not occur in our case, because there is a two-material composite and both the matrix and fiber materials are isotropic (Benveniste et al. [25]). It is worth mentioning that the partial strain concentration tensor $B^f_{\vec{p}}$ here explicitly depends on volume fraction, unlike the classical (analytical) MT model, because in the latter, $B^f_{\vec{p}}$ equals Eshelby's strain concentration tensor for a single ellipsoidal inhomogeneity embedded in an infinite matrix body.

3.4. Comparison between direct RVE and two-step homogenization results

For numerical simulations, we consider that the fibers obey an orientation tensor (OT) $\boldsymbol{a}$ which is supposed to have in a 2D case two non-zero components a_{11}=a and a_{22}=1-a:

$$[a] = \begin{bmatrix} a & 0 \\ 0 & 1 - a \end{bmatrix} \tag{19}$$

The following 2D orientation distribution function (ODF) is used, based on the "Natural closure approximation" proposed by Verleye et Dupret [23]

$$\Psi(\phi) = \frac{\frac{1}{2\pi}}{\frac{1-a}{a}(\cos\phi)^2 + \frac{a}{1-a}(\sin\phi)^2} \tag{20}$$

It is emphasized that in the current study, the micromechanical models are based on the ODF itself and not the OT. As shown by Müller and Böhlke [10] the sole use of the second-order OT is not sufficient and might lead to considerable errors in homogenization. Any ODF could be used in the current work The advantage of the Verleye-Dupret ODF is that it includes explicitly OT components, which are in practice the only orientation input available. Therefore there is no need to reconstruct an ODF from the OT. The ODF is depicted in figure 13 for various values of OT component a. For numerical simulations, the ODF is discretized for ϕ in [0,180] degrees and for various values of a. The weight of each discrete orientation ϕ_i is computed as : $w_i = 2\Psi(\phi_i)\Delta\phi$.
The predictions of four methods are compared: direct RVE-FE (section 3.2) and two-step FE-Voigt, FE-Reuss and FE-MT (section 3.3).

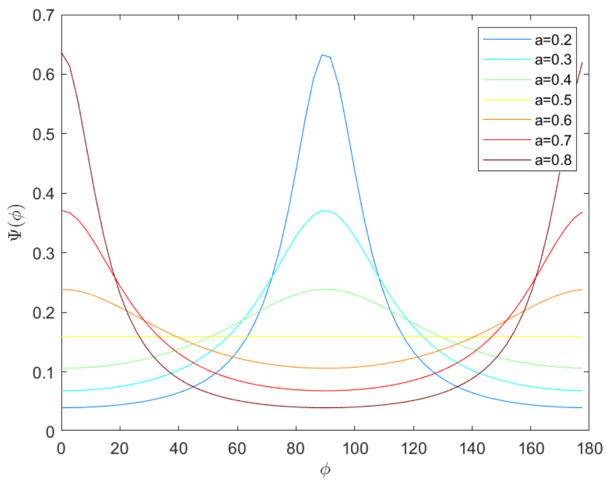

Figure 13: The curve of the ODF for each value of OT component a.

For the apparent Young's modulus along the X-direction as a function of the OT component a, figures 14 and 15 show for $v_f = 10\%$ and $v_f = 16\%$ that both two-step methods FE-MT and FE-Voigt give very similar results, which agree well with the reference direct FE simulations of RVE although a few predictions of FE-MT exceed slightly those of FE-Voigt. We note also that a few RVE-FE results are unexpectedly above the FE-Voigt estimates.
Regarding the apparent Young's modulus along the Y direction versus OT component a, figures 16 ($v_f = 10\%$) and 17 ($v_f = 16\%$) show that FE-Voigt and FE-MT give again very similar predictions, although their accuracy with respect to RVE-FE decreases, especially for $v_f = 16\%$. This time, all RVE-FE results are situated between the FE-Voigt and FE-Reuss estimates.
As for the apparent shear modulus in the (X, Y) plane, the observations are similar to those for the Y-direction apparent Young's modulus; see figures 18 ($v_f = 10\%$) and 19 ($v_f = 16\%$).

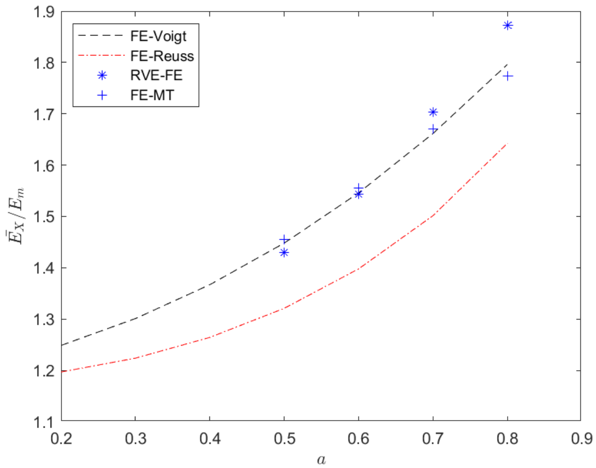

Figure 14: Misaligned fibers: Predictions of normalized $\overline{E}_X$ versus OT parameter a for $v_f = 10\%$.

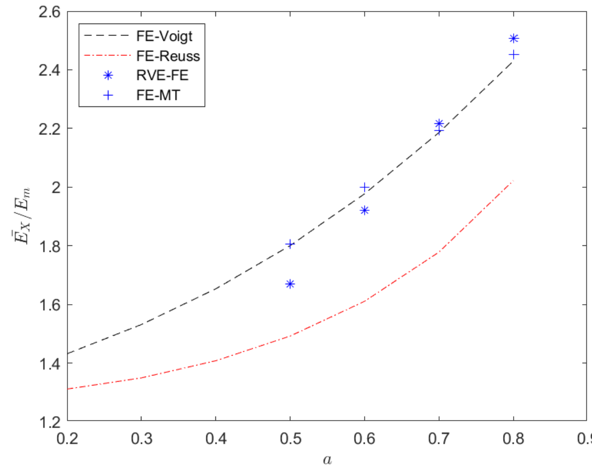

Figure 15: Misaligned fibers: Predictions of normalized $\overline{E}_X$ versus OT parameter a for $v_f = 16\%$.

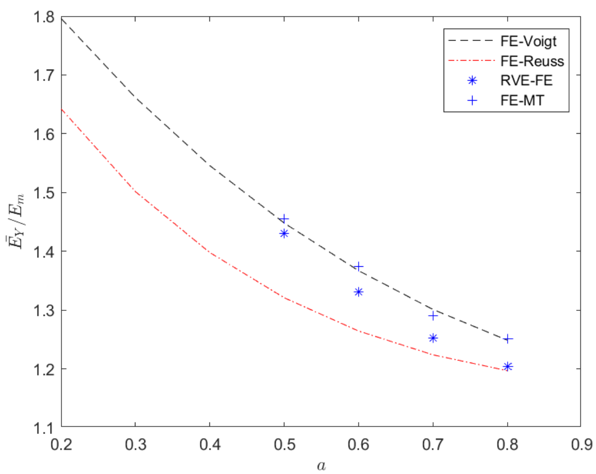

Figure 16: Misaligned fibers: Predictions of normalized $\overline{E}_Y$ versus OT parameter a for $v_f = 10\%$.

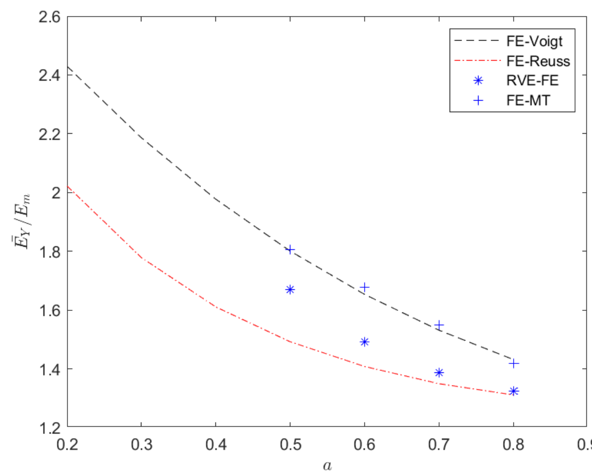

Figure 17: Misaligned fibers: Predictions of normalized $\bar{E}_Y$ versus OT parameter a for $v_f = 16\%$.

3.5. Strains inside the fibers

For a better evaluation of two-step methods, we compared mean strains inside individual fibers. In the first step, the stiffness matrix for a UD unit cell is computed by FE and in the second step we apply either Voigt (FE-Voigt) or direct MT (FE-MT) in order to compute the fibers' mean strain; see Appendix A for details. Figures 20, 21, and 22 show results inside fibers of orientation angles $\phi = 0, 15, 30, 45, 60$ degrees for three tests: a tension test along the X direction, another along the Y direction and a shear test. Figure 20 shows that $< \varepsilon_{XX} >_{\omega^f_{\vec{p}}}$ using FE-Voigt or FE-MT after applying a tension test along the X direction are very similar, for all orientation angles. The same observation holds for $< \varepsilon_{YY} >_{\omega^f_{\vec{p}}}$ (tension test in the Y direction) and $< \varepsilon_{XY} >_{\omega^f_{\vec{p}}}$ (shear test), figures 21 and 22. The FE-Voigt and FE-MT results are reasonably close to the RVE ones except in some cases. For uniaxial

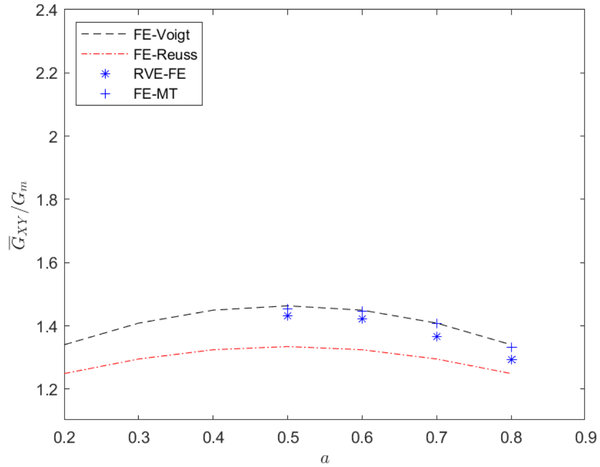

Figure 18: Misaligned fibers: Predictions of normalized $\bar{G}_{XY}$ versus OT parameter a for $v_f = 10\%$.

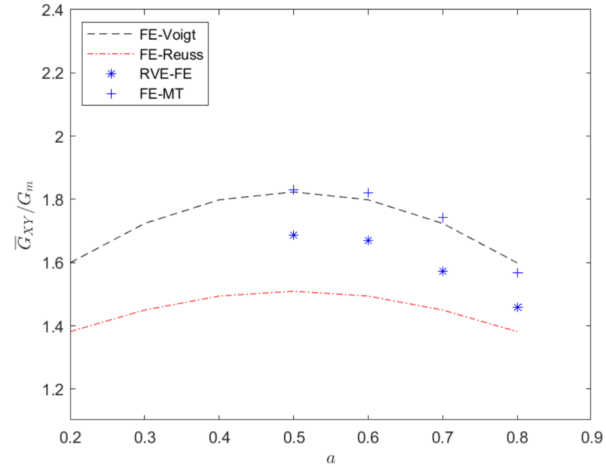

Figure 19: misaligned fibers: Predictions of normalized $\bar{G}_{XY}$ versus OT parameter a for $v_f = 16\%$.

tension, disagreement with RVE-FE is important for fibers fully or mostly aligned with the load direction($\phi = 0°$ and $\phi = 15°$ in fig. 20; $\phi = 45°$ and $\phi = 60°$ in fig. 21) . For shear test similar observation holds if we consider that the load is macroscopically equivalent to biaxial tension-compression at $\pm 45°$ ($\phi = 45°$ in Fig. 22).
To investigate further, we computed the strains inside the fibers at $\phi = 0°$ and compared them to the UD unit cell case. Table 6 shows that the UD unit cell results agree well with FE-Voigt and FE-MT, but the 3 results disagree with the RVE-FE. One reason for the disagreement is the difference between the fibers shapes which is rectangular in the unit cell and ellipsoidal in the RVE. Similarly to the fully aligned case(Sect.2) the fiber shape difference has an important impact on local results(local stresses and strains) and much less so on effective properties(obtained from volume averaging of local stress and strain fields.)

	FE-MT	FE-Voigt	RVE-FE	UD unit cell
$\frac{\varepsilon_{XX}}{\bar{\varepsilon}_{XX}}$	0.556	0.536	0.448	0.537

Table 6: Normalized strains inside the horizontal fibers for a tension test in the X direction and $v_f = 16\%$, OT parameter $a = 0.7$ for FE-MT, FE-Voigt and RVE-FE.

4. Conclusion

The main objective of this work was to conduct an unbiased evaluation of several homogenization strategies for misaligned SFRC. The focus was on the mostly used homogenization methods which are direct MT, on the one hand, and PG decomposition followed by two-step homogenization, on the other hand. However, in order to assess the strategies and conduct an unbiased evaluation, the investigation did not use analytical MF models, and relied only

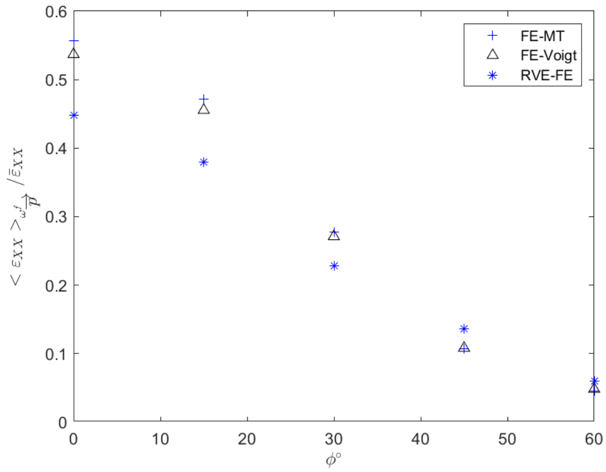

Figure 20: Misaligned fibers. Tension test along the X-direction. Predictions of normalized mean strain $< \varepsilon_{XX} >_{\omega^f_{\vec{p}}}$ inside the fibers of orientation angle ϕ for $v_f = 16\%$ and OT component $a = 0.7$.

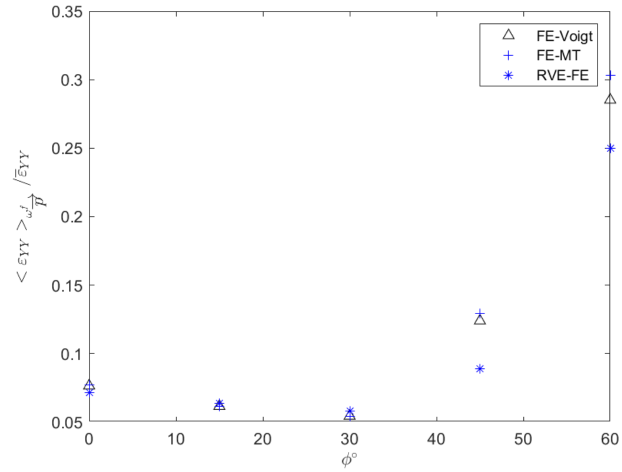

Figure 21: Misaligned fibers. Tension test along the Y-direction. Predictions of normalized mean strain $< \varepsilon_{YY} >_{\omega^f_{\vec{p}}}$ inside the fibers of orientation angle ϕ for $v_f = 16\%$ and OT component $a = 0.7$.

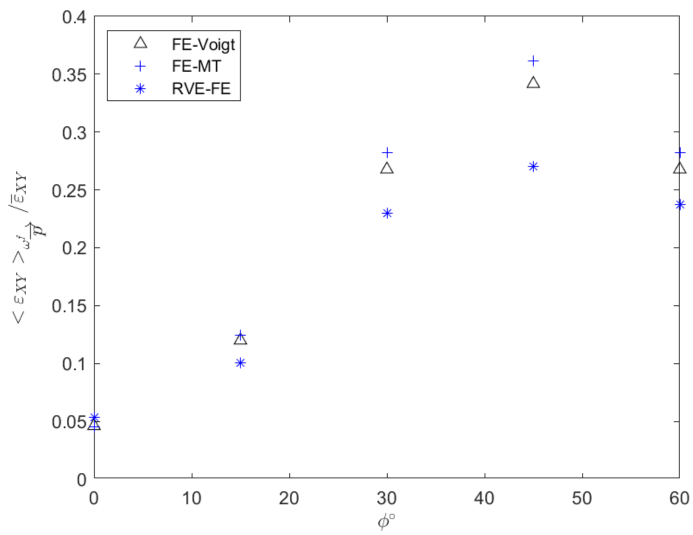

Figure 22: Misaligned fibers. Shear test. Predictions of normalized mean strain $< \varepsilon_{XY} >_{\omega^f_{\vec{p}}}$ inside the fibers of orientation angle ϕ for $v_f = 16\%$ and OT component $a = 0.7$.

on full-field FE calculations. Even the direct MT model was reformulated using only FE computations. This represents one of the original aspects of this work.

Since the building block of the homogenization models is a two-phase composite with UD fibers, we began by evaluating the accuracy of a simple UD unit cell as compared to an RVE with a large number of randomly located but aligned fibers. The simulations show that there is an excellent agreement in the predictions of the effective properties between the RVE and the unit cell, which proved the worth of the latter. Local strain and stress predictions are quite different. However computations showed that rule of mixture and especially a Voigt assumption in the fiber direction are not valid. A comparison was also made between the predictions of two 3D unit cells and 2D unit cells in plane stress or strain.

For misaligned fibers, we first performed FE homogenization of actual RVEs, to serve as reference results. Next, we implemented and compared three homogenization methods based on PG decomposition followed by two-step homogenization: FE-Voigt, FE-Reuss and FE-MT. The latter was shown to be equivalent to direct MT. In all cases, the homogenization of each PG is obtained by full-field FE on UD unit cells.

The results showed that FE-Voigt and FE-MT predict apparent engineering properties which are in a reasonable agreement with the reference results obtained by full-field FE directly on the actual RVEs. Similar conclusions hold for the predictions of the mean strains inside individual fibers, although a strong discrepancy between RVE-FE on the one hand, and FE-Voigt and FE-MT on the other hand, are observed for fibers aligned fully or partially with the load.

The simulations showed that two methods: (i) direct MT (i.e., FE-MT in this paper) and (ii) two-step homogenization with Voigt in the second step (i.e., FE-Voigt) lead basically to the same results in terms of effective properties and also of mean strains inside individual fibers. This may come as a surprise, since Jain et al. [7] for instance estimate that direct MT is better and should be the "standard (first choice) mean field homogenization method ". However, as we recalled in this paper, direct MT is just a special case of the method of PG decomposition and two-step homogenization. Also, Jain et al. [7] estimate that with two-step homogenization with Voigt in the second step: " interactions between dissimilar inclusions are lost ". However, this is the case even with direct MT, because all inclusions which have the same shape, aspect ratio, orientation and material are treated the same, regardless of where they are in the real RVE. Even with direct MT, instead of homogenizing the real RVE, one in fact computes a model RVE, which is in essence decomposed into PGs, each being a two-phase UD composite (see Fig. 1). Now since our parametric study of misaligned SFRC was limited to 2D microstructures, it is possible that a comprehensive investigation in 3D might conclude that FE-Voigt and FE-MT give different results, and that one method is to be preferred to the other.

In this work, we considered data typical of thermoplastic polymers reinforced with short glass fibers. Hence, the contrast between the Young's moduli of fibers and matrix was kept constant at 24.5 and the fibers' aspect ratio was fixed as 24. Also, most of the computations were performed in 2D. Therefore, it is possible that a more comprehensive parametric study might lead to some findings and conclusions which are different from the present ones. Instead of or in addition to direct MT estimates, future work should consider bounds of the Hashin-Shtrikman (HS) type, which are derived from a variational formulation and provide tight bounds for the effective stiffness. For misaligned short fibers embedded in a matrix, the MT estimates do not coincide with HS bounds. The latter can be estimated by the method of e.g. Lobos Fernández and Böhlke [9].

The current study is transferable to linear thermoelasticity, with the necessary changes brought by the strain concentration tensors in this situation (e.g., Pierard et al. [4]). Another extension which is the subject of current work is the introduction of a third phase, namely porosity. Other extensions of the present work are significantly challenging but are needed for a more realistic modeling of short fiber reinforced thermoplastics. Indeed, the response of a thermoplastic polymer matrix is nonlinear, and damage can initiate and evolve; e.g., (Kammoun et al. [5]), (Shokrieh and Moshrefzadeh-Sani [31]). The fibers' length is not fixed but distributed, and the fibers' orientation distributions differ between skin and core layers; e.g. (Muller et al. [29]), (Tseng et al. [30]). The complex microstructure can be captured by micro-computed tomography, e.g. Hessmann et al. [11]. Taking into account residual strains or stresses is another issue which needs to be addressed.

A. Appendix A: Two-step homogenization based on FE analysis of UD pseudo-grains (PGs)

A.1. PG level

Each PG is a two-phase composite made of identical and aligned fibers of orientation $\overrightarrow{p}$ embedded in a matrix. Strain concentration tensor $\boldsymbol{A}^f_{\overrightarrow{p}}$ and partial strain concentration tensor $\boldsymbol{B}^f_{\overrightarrow{p}}$ are defined such that (Dvorak and Benveniste, [25]):

$$< \boldsymbol{\varepsilon} >_{\omega^f_{\overrightarrow{p}}} = \boldsymbol{A}^f_{\overrightarrow{p}} :< \boldsymbol{\varepsilon} >_{\omega_{\overrightarrow{p}}} = \boldsymbol{B}^f_{\overrightarrow{p}} :< \boldsymbol{\varepsilon} >_{\omega^m_{\overrightarrow{p}}} \tag{A.1}$$

where $< \boldsymbol{\varepsilon} >_{\omega_{\overrightarrow{p}}}$, $< \boldsymbol{\varepsilon} >_{\omega^f_{\overrightarrow{p}}}$ and $< \boldsymbol{\varepsilon} >_{\omega^m_{\overrightarrow{p}}}$ designate the mean strain values over domains of the PG, the fibers and the matrix within the PG, resp. The concentration tensors are related :

$$\boldsymbol{A}^f_{\overrightarrow{p}} = \boldsymbol{B}^f_{\overrightarrow{p}} : (v_m \boldsymbol{I} + (1 - v_m)\boldsymbol{B}^f_{\overrightarrow{p}})^{-1};\ \boldsymbol{B}^f_{\overrightarrow{p}} = v_m(\boldsymbol{I} - (1 - v_m)\boldsymbol{A}^f_{\overrightarrow{p}})^{-1} : \boldsymbol{A}^f_{\overrightarrow{p}} \tag{A.2}$$

The effective stiffness $\overline{\boldsymbol{C}}_{\overrightarrow{p}}$ of the PG is such that :

$$< \boldsymbol{\sigma} >_{\omega_{\overrightarrow{p}}} = \overline{\boldsymbol{C}}_{\overrightarrow{p}} :< \boldsymbol{\varepsilon} >_{\omega_{\overrightarrow{p}}} \tag{A.3}$$

It can be expressed in terms of $\boldsymbol{A}^f_{\overrightarrow{p}}$ or $\boldsymbol{B}^f_{\overrightarrow{p}}$:

$$\begin{aligned} \overline{\boldsymbol{C}}_{\overrightarrow{p}} &= \boldsymbol{C}^m + (1 - v_m)(\boldsymbol{C}^f - \boldsymbol{C}^m) : \boldsymbol{A}^f_{\overrightarrow{p}} \\ &= (v_m \boldsymbol{C}^m + (1 - v_m)\boldsymbol{C}^f : \boldsymbol{B}^f_{\overrightarrow{p}}) : (v_m \boldsymbol{I} + (1 - v_m)\boldsymbol{B}^f_{\overrightarrow{p}})^{-1} \end{aligned} \tag{A.4}$$

In this paper $\overline{\boldsymbol{C}}_{\overrightarrow{p}}$ is computed by FE analysis on the (UD) PG and $\boldsymbol{A}^f_{\overrightarrow{p}}$ and $\boldsymbol{B}^f_{\overrightarrow{p}}$ can then be retrieved from $\overline{\boldsymbol{C}}_{\overrightarrow{p}}$ (see also Mayes and Hansen, [28]):

$$\begin{aligned} \boldsymbol{A}^f_{\overrightarrow{p}} &= \frac{1}{1 - v_m}(\boldsymbol{C}^f - \boldsymbol{C}^m)^{-1} : (\overline{\boldsymbol{C}}_{\overrightarrow{p}} - \boldsymbol{C}^m); \\ \boldsymbol{B}^f_{\overrightarrow{p}} &= \frac{v_m}{1 - v_m}(\boldsymbol{C}^f - \overline{\boldsymbol{C}}_{\overrightarrow{p}})^{-1} : (\overline{\boldsymbol{C}}_{\overrightarrow{p}} - \boldsymbol{C}^m) \end{aligned} \tag{A.5}$$

A.2. Two-step homogenization and direct Mori-Tanaka(MT)

Consider a RVE of domain ω made of misaligned fibers embedded in a matrix. The fibers are identical and their orientation distribution function (ODF) is $\Psi(\overrightarrow{p})$. Assuming that the RVE can be seen as an aggregate of PGs made of UD fibers embedded in a matrix,

$$\begin{aligned} < \boldsymbol{\varepsilon} >_\omega &= v_m < \boldsymbol{\varepsilon} >_{\omega^m} + (1 - v_m)\langle < \boldsymbol{\varepsilon} >_{\omega^f_{\overrightarrow{p}}} \rangle_\Psi \ ; \\ < \boldsymbol{\sigma} >_\omega &= v_m \boldsymbol{C}^m :< \boldsymbol{\varepsilon} >_{\omega^m} + (1 - v_m)\langle \boldsymbol{C}^f :< \boldsymbol{\varepsilon} >_{\omega^f_{\overrightarrow{p}}} \rangle_\Psi \end{aligned} \tag{A.6}$$

where ω^m is the matrix domain in the RVE and $< . >_\Psi$ is an orientation averaging over all PGs, weighted with the ODF $\Psi(\overrightarrow{p})$. As shown by Pierard et al. [4], a direct MT model can be seen as a two-step method where the following assumption is made :

$$< \boldsymbol{\varepsilon} >_{\omega^m_{\overrightarrow{p}}} = < \boldsymbol{\varepsilon} >_{\omega^m}, \ \forall \overrightarrow{p} \tag{A.7}$$

Consequently, for direct MT, strain concentration tensor $\boldsymbol{B}^f_{\overrightarrow{p}}$ is such that:

$$< \boldsymbol{\varepsilon} >_{\omega^f_{\overrightarrow{p}}} = \boldsymbol{B}^f_{\overrightarrow{p}} :< \boldsymbol{\varepsilon} >_{\omega^m} \tag{A.8}$$

Therefore, the RVE's stiffness $\overline{\boldsymbol{C}}$ defined as:

$$< \bar{\sigma} >_\omega = \overline{\boldsymbol{C}} :< \boldsymbol{\varepsilon} >_\omega \tag{A.9}$$

is estimated by Mori-Tanaka as :

$$\overline{\boldsymbol{C}}^{MT} = (v_m \boldsymbol{C}^m + (1 - v_m) < \boldsymbol{C}^f : \boldsymbol{B}^f_{\overrightarrow{p}} >_\Psi) : (v_m \boldsymbol{I} + (1 - v_m) < \boldsymbol{B}^f{}_{\overrightarrow{p}} >_\Psi)^{-1} \tag{A.10}$$

One can check that a direct MT method, formulated without PG decomposition and two-step method, leads indeed to the same expression of $\overline{\boldsymbol{C}}^{MT}$. In this paper analytical formulae for MT are not used and $\boldsymbol{B}^f_{\overrightarrow{p}}$ is computed for the FE evaluation of $\overline{\boldsymbol{C}}_{\overrightarrow{p}}$ (sect.A.1)

A.3. Strains and stresses in the fibers with the two-step method

The FE-Voigt method uses FE in the first step and Voigt hypothesis in the second step

$$< \boldsymbol{\varepsilon} >_{\omega_{\overrightarrow{p}}} = < \boldsymbol{\varepsilon} >_\omega, \ \forall \overrightarrow{p} \tag{A.11}$$

Therefore strain concentration $\boldsymbol{A}^f_{\overrightarrow{p}}$ is such that

$$< \boldsymbol{\varepsilon} >_{\omega^f_{\overrightarrow{p}}} = \boldsymbol{A}^f_{\overrightarrow{p}} :< \boldsymbol{\varepsilon} >_\omega \tag{A.12}$$

We recall that in this paper $\overline{\boldsymbol{C}}_{\overrightarrow{p}}$ is computed by FE analysis, and $\boldsymbol{A}^f_{\overrightarrow{p}}$ is retrieved from $\overline{\boldsymbol{C}}_{\overrightarrow{p}}$ thanks to equ.(A.5)
As for FE-MT, which is equivalent to direct MT, the first step is also obtained by FE, and the second step corresponds to the following hypothesis

$$< \boldsymbol{\varepsilon} >_{\omega^f_{\overrightarrow{p}}} = \boldsymbol{B}^f_{\overrightarrow{p}} :< \boldsymbol{\varepsilon} >_{\omega^m} \tag{A.13}$$

Combining this equation with equ.(A.6) it is found that:

$$< \boldsymbol{\varepsilon} >_{\omega^f_{\overrightarrow{p}}} = \boldsymbol{B}^f_{\overrightarrow{p}} : (v_m \boldsymbol{I} + (1 - v_m) < \boldsymbol{B}^f_{\overrightarrow{p}} >_\Psi)^{-1} :< \boldsymbol{\varepsilon} >_\omega \tag{A.14}$$

Again we emphasize that analytical formulae for MT are not used and $\boldsymbol{B}^f_{\overrightarrow{p}}$ is computed from the FE estimate of $\overline{\boldsymbol{C}}_{\overrightarrow{p}}$ (equ.(A.5)).

5. References

[1] C. W. Camacho, C. L. Tucker, S. Yalvac, and R. L. McGee. Stiffness and thermal expansion predictions for hybrid short fiber composites Polymer Composites Volume 11, Issue 4, August 1990, Pages 229-239.

[2] Lielens, G., 1999. Micro–macro modeling of structured materials. Ph.D. Thesis, Université Catholique de Louvain, Belgium

[3]H.R. Lusti, A.A. Gusev Finite element predictions for the thermoelastic properties of nanotube reinforced polymers, Model. Simul. Mater. Sci. Eng., 12 (2004), p. S107

[4] O. Pierard, C. Friebel, and I. Doghri. Mean-field homogenization of multi-phase thermo-elastic composites : A general framework and its validation. Composites Science and Technology, 64 (10-11) :1587-1603, 2004.

[5]Kammoun, S., I-Doghri, Brassart, L., Delannay,L., Micromechanical modeling of the progressive failure in short glass-fiber reinforced thermoplastics - First Pseudo-Grain Damage model, Composites Part A: Applied Science and Manufacturing A 73 (2015), 166-175.

[6] T. Mori and K. Tanaka. Average stress in matrix and average elastic energy of materials with misfitting inclusions. Acta metallurgica, 21(5) :571-574, 1973.

[7] Jain, A., Lomov, S.V., Abdin, Y., Verpoest, I., Van Paepegem, W., 2013. Pseudo-grain discretization and full Mori Tanaka formulation for random heterogeneous media: Predictive abilities for stresses in individual inclusions and the matrix. Composites Science and Technology 87, 86–93.

[8] Müller, V., Kabel, M., Andrä, H., Böhlke, T., 2015. Homogenization of linear elastic properties of short-fiber reinforced composites – A comparison of mean field and voxel-based methods. International Journal of Solids and Structures 67–68, 56–70.

[9] Lobos Fernández, M., Böhlke, T.: Representation of Hashin-Shtrikman bounds in terms of texture coefficients for arbitrarily anisotropic polycrystalline materials. Journal of Elasticity, 1-38 (2018).

[10] V. Müller, T. Böhlke, Prediction of effective elastic properties of fiber reinforced composites using fiber orientation tensors. Composites Science and Technology; 130 (2016) 36-45.

[11] P. A. Hessman, T. Riedel, F. Welschinger, K. Hornberger, T. Böhlke, Microstructural analysis of short glass fiber reinforced thermoplastics based on x-ray micro-computed tomography. Composites Science and Technology S0266-3538, 2019.

[12] Tian, W., Qi, L., Liang, J., Chao, X., Zhou, J., 2016a. Evaluation for elastic properties of metal matrix composites with randomly distributed fibers: Two-step mean-field homogenization procedure versus FE homogenization method. Journal of Alloys and Compounds 658, 241–247.

[13] Tian, W., Qi, L., Su, C., Liang, J., Zhou, J., 2016b. Numerical evaluation on mechanical properties of short-fiber-reinforced metal matrix composites: Two-step mean-field homogenization procedure. Composite Structures 139, 96–103.

[14] Digimat, 2018. Linear and nonlinear multi-scale material modeling software, e-Xstream engineering SA, Louvain-la-Neuve, Belgium. Available from: http://www.e-Xstream.com.

[15] Leclerc, W., Karamian-Surville, P., 2013. Effects of fibre dispersion on the effective elastic properties of 2D overlapping random fibre composites. Comput. Mater. Sci. 79, 674â683.

[16] Harper, L.T., Qian, C., Turner, T.A., Li, S., Warrior, N.A., 2012. Representative volume elements for discontinuous carbon fibre composites â Part 1: Boundary conditions. Compos. Sci. Technol. 72, 225â234.

[17] Abaqus. A general-purpose finite element program, RI, USA.

[18] Lippmann, N., Steinkopff, T., Schmauder, S., Gumbsch, P., 1997. 3D-finite-element-modelling of microstructures with the method of multiphase elements. Comput. Mater. Sci., Selected papers of the Sixth International Workshop on Computational Mechanics of Materials 9, 28–35.

[19] Kanit, T., Forest, S., Galliet, I., Mounoury, V., Jeulin, D., 2003.Determination of the size of the representative volume element for random composites: statistical and numerical approach. Int. J. Solids Struct. 40, 3647–3679.

[20] Kang G.Z, Q. Gao. Tensile properties of randomly oriented short $\delta - Al_2O_3$ fiber reinforced aluminum alloy composites : II. Finite element analysis for stress transfer, elastic modulus and stress-strain curve. Composites Part A : Applied Science and Manufacturing, 33(5) :657-667,2002.

[21] H. J. Bohm. A Short Introduction To Basic Aspects Of Continuum Micromechanics. 2011.

[22] Y. Benveniste. A new approach to the application of Mori-Tanaka's theory in composite materials.Mechanics of materials, 6(2) :147-157, 1987.

[23] F. Dupret and V. Verleye. Modelling the flow of fiber suspensions in narrow gaps, in advances in the flow and rheology of non-newtonian fluids, rheology series, 8, 1999.

[24]Levy A., Papazian J.M.: Elastoplastic Finite Element Analysis of Short-Fiber-Reinforced SiC/Al Composites: Effects of Thermal Treatment; Acta metall.mater.39, 2255–2266, 1991.

[25]Benveniste,Y., G.J Dvorak, T. Chen. On diagonal and elastic symmetry of the approximate effective stiffness tensor of heterogeneous media, J. Mech. Phys. Solids, vol. 39, no. 7, 927-946 (1991).

[26]I. Balberg, N. Binenbaum, and N. Wagner. Percolation Thresholds in the Three-Dimensional Sticks System, Phys. Rev. Lett. 52, 1465, 1984

[27]Dvorak, G.J., Y.Benveniste. On transformation strains and uniform fields in multiphase elastic medi, Proc. R. Soc. London A (1992) 437, 291-310.

[28]Mayes, J.S., A.C. Hansen. Multicontinuum Failure Analysis of Composite Structural Laminates, Mechanics of Composite Materials and Structures, 8:4,249-262.

[29]Müller, V., Brylka, B., Dillenberger, F., Glöckner, F.,R, Kolling, S., Böhlke, T. Homogenization of elastic properties ofshort-fiber reinforced composites based on measured microstructure data, Journal of composite materials, 50(3) 297–312, 2016.

[30]Tseng, H.-C., Chang, R.-Y, Hsu, C.-H, Numerical prediction of fiber orientation and mechanical performance for short/long glass and carbon fiber-reinforced composites, Composites Science and Technology, 144, 51-56, 2017.

[31]Shokrieh, M.M., Moshrefzadeh-Sani, H., A novel laminate analogy to calculate the strength of two-dimensional randomly oriented short-fiber composites, Composites Science and Technology 147 (2017) 22-29.